Isotope-selective laser ablation ion-trap loading of $^{137}Ba^+$ using a $BaCl_2$ target

Brendan M. White, Pei Jiang Low, Yvette de Sereville, Matthew L. Day, Noah Greenberg, Richard Rademacher, and Crystal Senko*
Department of Physics and Astronomy, University of Waterloo, Waterloo, N2L 3R1 Canada and Institute for Quantum Computing, University of Waterloo, Waterloo, N2L 3R1 Canada

(Received 18 October 2021; accepted 11 February 2022; published 9 March 2022)

The $^{133}Ba^+$ ion is a promising candidate as a high-fidelity qubit, and the $^{137}Ba^+$ isotope is promising as a high-fidelity qudit ($d > 2$). Barium metal is very reactive, and $^{133}Ba^+$ is radioactive and can only be sourced in small quantities, so the most commonly used loading method, oven heating, is less suited for barium and is currently not possible for $^{133}Ba^+$. Pulsed laser ablation solves both of these problems by utilizing compound barium sources while also giving some distinct advantages, such as fast loading, less displaced material, and lower heat load near the ion trap. Because of the relatively low abundances of the isotopes of interest, a two-step photoionization technique is used, which gives us the ability to selectively load isotopes. Characterization of the ablation process for our $BaCl_2$ targets are presented, including observation of neutral and ion ablation-fluence regimes, preparation and conditioning, lifetimes of ablation spots, and plume velocity distributions. We show that by using laser ablation on $BaCl_2$ salt targets with a two-step photoionization method, we can produce and trap barium ions reliably. Furthermore, we demonstrate that with our photoionization method, we can trap $^{137}Ba^+$ with an enhanced selectivity compared to its natural abundance.

DOI: 10.1103/PhysRevA.105.033102

I. INTRODUCTION

Ion traps have been studied extensively as a promising platform for quantum computing [1,2]. Trapped ions as qubits have been demonstrated with many different elements [3–13], and the barium isotopes, $^{133}Ba^+$ and $^{137}Ba^+$, show much promise for high-dimensional quantum information [9,14,15]. However, barium presents some unique difficulties as an atomic source because of its metal form's chemical properties and $^{133}Ba^+$ sourcing limitations. To use these isotopes for quantum information, a reliable method must be developed for selectively trapping specific isotopes using barium-salt targets. In this paper, we describe such a method which uses ablation and two-step photoionization. We carefully characterize the process of preparing our ablation targets and present quantitative selectivity enhancement results. Furthermore, we investigate the ablation dynamics from barium-salt targets and observe a surprisingly large plume temperature.

Loading ions into an ion trap requires the generation of a flux of the desired atoms through the center of the trap along with a method to ionize the atoms. The most commonly used method for generating the atomic flux is Joule heating of an oven source [4,16–23].

In recent years, laser ablation has become a more common method for loading ions [14,24,25]. This method uses a pulsed laser with a high pulse energy to ablate atoms from a source [26–30], and it can result in less contamination [31,32], a lower pressure rise at the trap center [31], and a lower overall heat load to the vacuum chamber [33]. The major disadvantage of ablation is the high variance of neutral flux from shot to shot and for different spots on a target. Compared to ovens, which require metal sources (excepting special setups [18]), the source target in laser ablation can be either a pure metal or a compound and requires less material. This amelioration solves the problem of generating ^{133}Ba atoms, which can only be obtained in microgram quantities (due to its radioactive properties) and is typically obtained in the form of a chemical compound, such as $BaCl_2$. Furthermore, ablation is useful for the element barium, in general [14,25,34], which, in metal form, oxidizes within seconds in air [18,22]. For these reasons, we focus on laser ablation in our experiment.

Using laser ablation, charged ions can be generated directly [14,25,26,32,35–44], or ablated neutral atoms can be ionized by electron-impact ionization [45–47]. Unfortunately, this method is significantly less efficient than other methods, such as photoionization [17,48], and neither of these ionization methods discriminate between different isotopes. Resonant photoionization [16,17,19–22,24,33,49–60] in which multiple lasers are used to excite a valence electron and then eject it completely is commonly used to selectively load ions. Isotope selectivity is important for applications like quantum computing, which require the deterministic loading of ten or more specific isotopes. This is a particularly salient point in the case of barium because of its large number of abundant naturally occurring isotopes.

In this paper, we use laser ablation to generate neutral-barium atoms and two-step photoionization to ionize them. We characterize ablation from a barium-salt target, describing the steps to prepare the target, and the best parameters we found for trapping ions consistently. A crucial step was "conditioning," where fresh spots on the target first needed to

*csenko@uwaterloo.ca

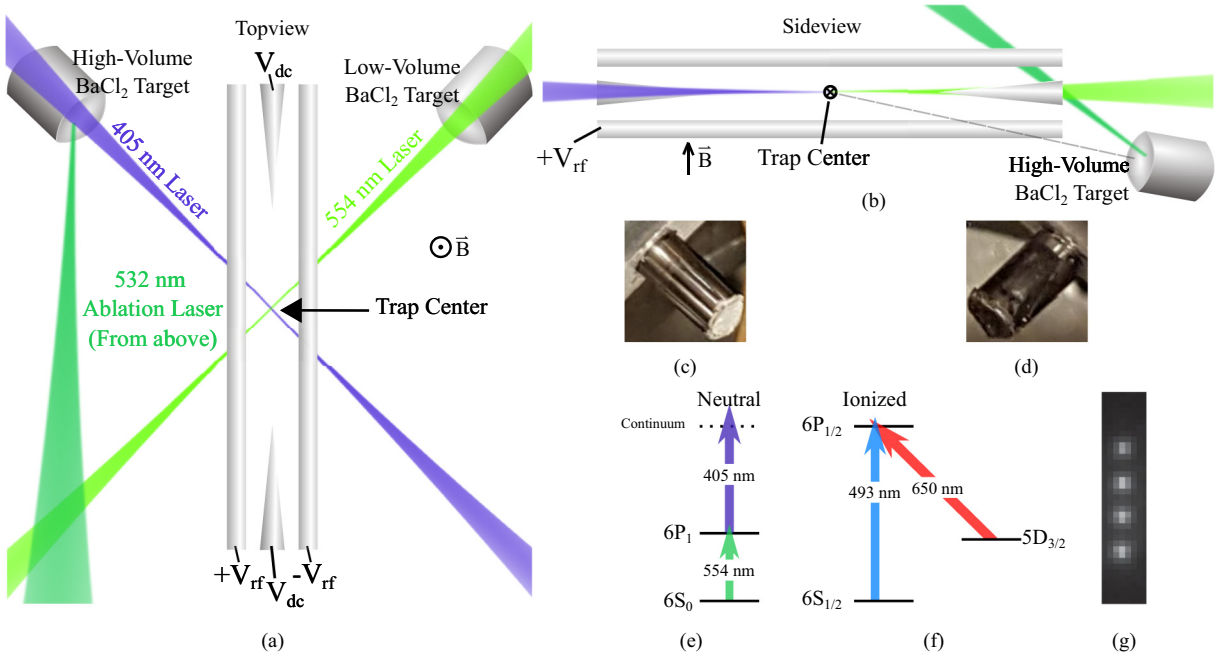

FIG. 1. (a) and (b) Experimental setup for laser ablation trapping. Ablation targets point directly towards the trap center. The ablation laser enters through the top view port. To use the low-volume target, the ionization beams' directions are swapped. (c) and (d) High- and low-density targets, respectively. (e) Relevant energy structure of neutral barium: A two-step photoionization process with 554- and 405-nm lasers [21,50,61–65] is used to eject a valence electron from neutral barium, ionizing it. (f) Relevant energy structure of ionized barium: a 493-nm laser drives the $S_{1/2} \leftrightarrow P_{1/2}$ transition to Doppler cool the ion and a 650-nm repump laser drives the $D_{3/2} \leftrightarrow P_{1/2}$ transition. These cooling lasers are co-propogating with the first-step photoionization (554-nm) laser. (g) A chain of four trapped $^{138}Ba^+$ ions with $\sim 13\,\mu$m distance between them.

be ablated with a high fluence before they gave a sufficient atomic flux using a lower fluence. We present results of time-resolved spectroscopy on the resonant step of photoionization, giving an estimation of the velocities of ablated atoms. We find that the ablation plume from a barium-salt target has a significantly higher temperature than that of metal targets. Finally, we demonstrate trapping of $^{137}Ba^+$, present loading rates, and show isotope selectivity for the ion of interest $^{137}Ba^+$. We also discuss results from a low-volume ablation target intended for trapping $^{133}Ba^+$, and we give a likely explanation for its insufficiency.

II. EXPERIMENT

The layout of our experiment is shown in Figs. 1(a) and 1(b). The ion trap is a four-rod Paul trap with needles as end caps [66]. Around 5–10 V is applied to the needles to confine ions axially. An rf voltage of $|V_{rf}| \approx 66$ V is applied to all four rods with each set of diagonal rods having opposite polarity to confine ions radially. The ablation targets are aluminum cylinders with recessed ends containing barium chloride ($BaCl_2$), which are mounted inside the vacuum chamber below the side view ports. The targets are angled directly towards the trap center, and the recessed surfaces are concave hemispheres radially matched to the distance to the trap center in order to maximize the flux of trappable atoms. The distance from the targets' surfaces to the trap center is 14.6 mm. The high-volume natural-abundance target (see Table I) is used as a source for most isotopes of barium, whereas the low-volume target is used as a source for ^{133}Ba.

Since barium metal oxidizes within seconds in air, we instead use barium salt. For the high-volume target, we mixed natural-abundance $BaCl_2$ with a small amount of de-ionized

TABLE I. Natural abundance and first-step photoionization transition frequencies of barium isotopes.

Isotope	Abundance	Isotope shift (MHz)[a]
132	0.1%	167.9
133[b]	0%	−23.3 ($J' = 1/2$) 373.8 ($J' = 3/2$)
134	2.4%	142.8
135	6.6%	547.3 ($J' = 5/2$) 326.7 ($J' = 3/2$) 121.6 ($J' = 1/2$)
136	7.9%	128.02
137	11.2%	549.5 ($J' = 5/2$) 326.7 ($J' = 3/2$) 63.4 ($J' = 1/2$)
138	71.7%	0

[a]Relative to ^{138}Ba transition.
[b]Radioactive isotopes need enriched targets. Odd isotopes have nonzero nuclear spin and different excited states J'.

water to form a paste, which we applied to the recessed end of the ablation target, giving a high-volume natural-abundance 30-mg $BaCl_2$ target. The low-volume target was made from a solution of hydrochloric acid (HCl), with approximately 0.4 mCi of ^{133}Ba. Because HCl corrodes aluminum, we fit a tantalum foil over the tube's end. To apply the solution to the target, we dropped 10 μL in the target cup (which is sitting on a 250 °C hotplate), let it evaporate, leaving 200 ng of $BaCl_2$ salt on the surface, and repeated this process until we had ∼10 μg on the substrate. With such a low volume, the deposited salt is imperceptible on the substrate tantalum foil [see Figs. 1(c) and 1(d)].

To ablate the targets, we use a Nd:YAG pulsed laser at wavelength 532 nm and a pulse width of 3–5 ns. We focus the ablation laser to a radius of 98 and 82 μm onto the high- and low-volume targets, respectively. With this beam size, we estimate that there are on the order of 500 distinguishable spots on the targets. The fluence is typically set from 0.2 to 0.5 J cm^{-2}. In this paper, data are collected from ablation of the high-volume target unless otherwise noted. The beam comes in from the top view port at 56° from the high- and low-volume target normals. Two servomotors on a mirror mount in the ablation-laser path allow for precisely moving the ablation laser or sweeping over an area during an experiment.

A two-step photoionization process, depicted in Fig. 1(e), is used to ionize ablated neutral atoms at the trap center. The first step uses a 553-nm laser to drive one of the valence electrons of neutral barium into the $^1P_1$ state. Since the first-step transition in neutral barium is resonant and has different frequencies for different isotopes, these peaks are discernible [50,61,62] for a sufficiently low laser linewidth. Therefore, in principle, this laser frequency can be varied to selectively ionize and load. This laser is oriented perpendicular to the flux of neutral atoms in order to minimize Doppler broadening and shifting. The second-step photoionization laser at 405 nm is oriented perpendicular to the first-step laser to restrict the volume of ionization to be near the trap center, minimizing the potential energy of ions that are trapped and reducing the cooling time for hot newly captured ions. The laser used to drive the first step of photoionization has a saturation power of $P_{\text{sat}} = 0.57\,\mu$W [67] (ionization lasers are focused at a 35-μm radius).

Upon being ionized, ions begin to fluoresce from the 493- and 650-nm lasers, which are both co-propogating with the 554-nm laser. The 493-nm laser is used to Doppler cool the ion and a 650-nm repump laser is used to repump out of the $5D_{3/2}$ state. Once the ion has been cooled sufficiently, it crystallizes in the center of the ion trap. Trapped ions are imaged with an imaging objective with a numerical aperture of 0.26.

The photons collected by the objective are read out using a photomultiplier tube (PMT) if the experiment requires measurement of the overall brightness of ions or using a complementary metal-oxide semiconductor camera to spatially discriminate between ions in a crystallized chain. The PMT can also be used to collect neutral fluorescence from an ablated neutral-atom (flux) or ion flux.

All data used for the results in this paper can be found in the repository in Ref. [68].

III. ABLATION CHARACTERIZATION

In this section, we describe preparation of fresh spots on the ablation target and the different regimes in which neutral atoms or ions are generated by ablation of our targets. Furthermore, we characterize spatial and temporal variations of atomic flux and the typical number of pulses in which a single spot will give a significant atomic flux through the trap center.

We assess the atomic flux of neutral (or singly ionized) barium atoms ablated through the trap center based on the fluorescence collected while the atoms transit through the 554- (or 493-nm) laser beam, respectively. The laser powers are set around 100–200× saturation, and the laser frequencies are set to the resonance frequencies of the $^{138}Ba^+$ isotope. Fluorescence is quantified by the number of PMT counts in a 55-μs time window beginning 3 μs after the ablation-laser pulse is incident on the ablation target. As shown in Fig. 4, this time window spans the majority of the observable neutral-fluorescence signal. Note that applying very high fluence on the order of 1 J/cm^2 results in an appreciable amount of excited-state neutral atoms (or other fluorescing material) passing through the trap center as discussed further in the Supplemental Material [69]. For all results reported in this paper, we use laser fluences well below the threshold where this confounding signal appears.

When aligned to a fresh spot on the target, no neutral-atom production is observed for fluences below 0.3 J/cm^2. With a higher fluence of 0.3 to 0.75 J/cm^2, neutral-atom fluorescence of 100–400 counts starts to be observed. Upon returning to low fluence, neutral-atom flux may then be observable. We call this process of applying high-fluence pulses with the purpose of activating neutral-atom production at low fluence conditioning. New spots do not always give observable neutral fluorescence at high fluence, and even ones that do are not guaranteed to produce a significant neutral-fluorescence signal at low laser fluence as shown later in this section. Conditioning can allow access to a regime in which neutral atoms are produced, but ionized atoms are not. As shown in Fig. 2, neutral atoms are generated with a fluence above 0.1 J/cm^2, whereas ions are generated above 0.25 J/cm^2. The data in Fig. 2 were collected while sweeping the ablation laser over a 300 × 700-μm^2 area which was previously conditioned with on the order of 100 pulses at 0.50 J/cm^2. Mean, maximum, and standard deviations are computed for data collected over two sweeps with 120 pulses per sweep. We observe that the ion-fluorescence signal is well correlated spatially with the vacuum-chamber pressure spikes. The neutral fluorescence plateaus near the onset of ions where there is much less spacial variation over the sweep than at lower fluence. In practice, it is desirable to use spots that produce neutral atoms below the ions regime to reduce excess charge buildup on electrodes and to more easily build chains of ions (see Sec. V). Because of the extreme variation during a sweep in this neutral-atom regime, the remaining data sets in this paper were collected with the ablation laser fixed on a single spot.

The conditioning process has highly variable outcomes (see Supplemental Material [69]), but three common behaviors emerged, illustrated in Fig. 3(a). In these experiments, each fresh spot was exposed alternately to ten conditioning pulses (0.48 J/cm^2) and ten low-fluence pulses (0.20 J/cm^2).

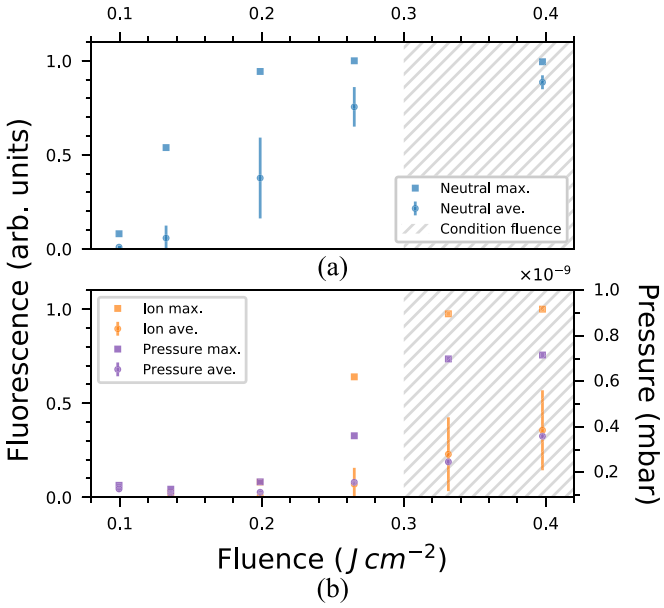

FIG. 2. Neutral-atom and ion production regimes. Diagonally hatched areas denote conditioning fluences. (a) Neutral-atom fluorescence vs pulse fluence. (b) Ion fluorescence and vacuum chamber pressure spikes vs pulse fluence.

The neutral fluorescence at low and conditioning fluences is plotted against the number of conditioning pulses for three spots exhibiting the most common behaviors. Out of 17 fresh spots near the target center (see the Supplemental Material [69] for the remaining data sets), five (29%) were high yield with over 50 counts, four (24%) were moderate yield with 10–50 counts, and eight (47%) were low yield, never exceeding ten counts. Typically, neutral-atom flux at low fluence plateaus after approximately 200 conditioning pulses. In a separate set of experiments, we observe that fluences below the threshold for ion production will not condition a fresh spot to produce neutral atoms even after several thousand pulses. We also observe that spots towards the edge of the target are much less likely to yield significant neutral-atom flux (see the Supplemental Material [69]).

Even for high-yield spots, there is significant temporal variation in the ablated atomic flux with the spot eventually giving no observable neutral-fluorescence signal. Therefore, an important metric is the lifetime of a single spot, i.e., the amount of pulses before the neutral-fluorescence signal reduces to near background. As shown in Fig. 3(b), using a fluence of $0.15\,\mathrm{J/cm^2}$ and a pulse repetition rate of 2 Hz, the average spot lifetime is ~10 000 pulses. Often, reconditioning a used-up spot revives it, but the lifetime after reconditioning is typically under 2000 pulses.

On the low-volume target, a much higher fluence of $0.6\,\mathrm{J/cm^2}$ is needed before neutral fluorescence is observable. This signal diminishes to background levels after just tens of pulses (see the Supplemental Material [69] for details). Contrary to the natural-abundance barium target, reconditioning an area where the atomic flux is reducing never restores it but instead speeds up the reduction. We interpret these observations, performed for several large sweeps, as indications that the ablation completely depletes the source of neutral barium

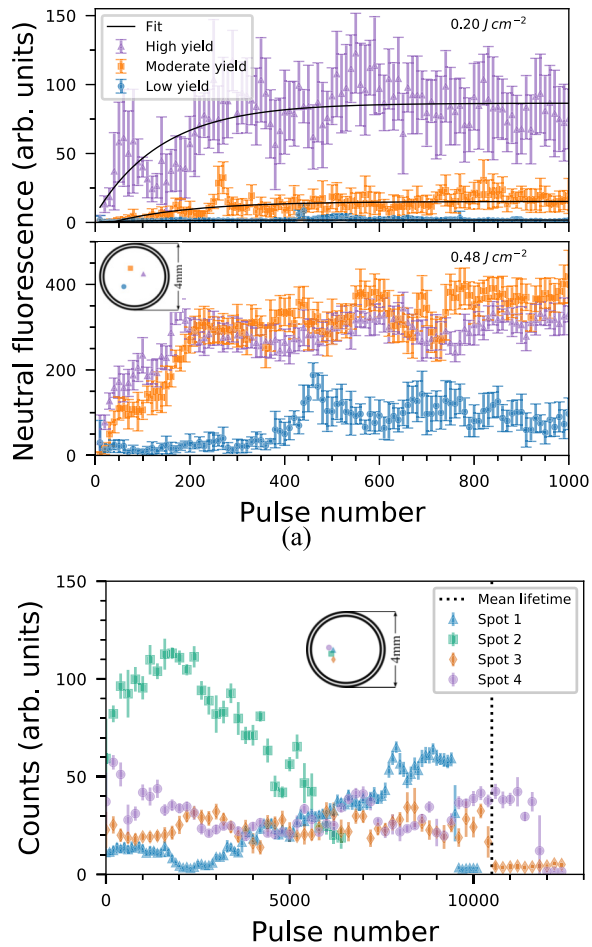

FIG. 3. Ablation spot lifetimes and conditioning. First-step photoionization laser power is $\sim 150 \times P_{\mathrm{sat}}$. The inset circles represent the target with the specific spots corresponding to the data labeled. (a) Low-fluence at $0.20\,\mathrm{J/cm^2}$ (top) and conditioning at $0.48\,\mathrm{J/cm^2}$ (bottom). At low-fluence, some spots were high yield, giving over 50 counts. Most spots gave a moderate yield with over 10 counts measured. The remaining spots were low yield, giving counts very near background. (b) Neutral fluorescence spot lifetime for several spots.

atoms. This is supported by observations with similarly prepared targets that laser ablation causes thin layers of $BaCl_2$ to fragment and flake off their substrate material.

IV. PLUME CHARACTERIZATION

Several characteristics of the ablated plume of neutral-barium atoms are illuminated by performing a time-resolved spectroscopy experiment [58] in which neutral-atom fluorescence is collected in 1-μs time bins for different first-step photoionization laser frequencies. From these data, we observe the Doppler shift of ablated atoms, generate a first-step photoionization spectrum showing resolved isotope peaks, and generate a velocity distribution.

The time-resolved spectrum is shown in Fig. 4(a). In this experiment, each point is the average of neutral fluorescence from five pulses, and each measurement is calibrated by a reference neutral-fluorescence measurement before and after it to

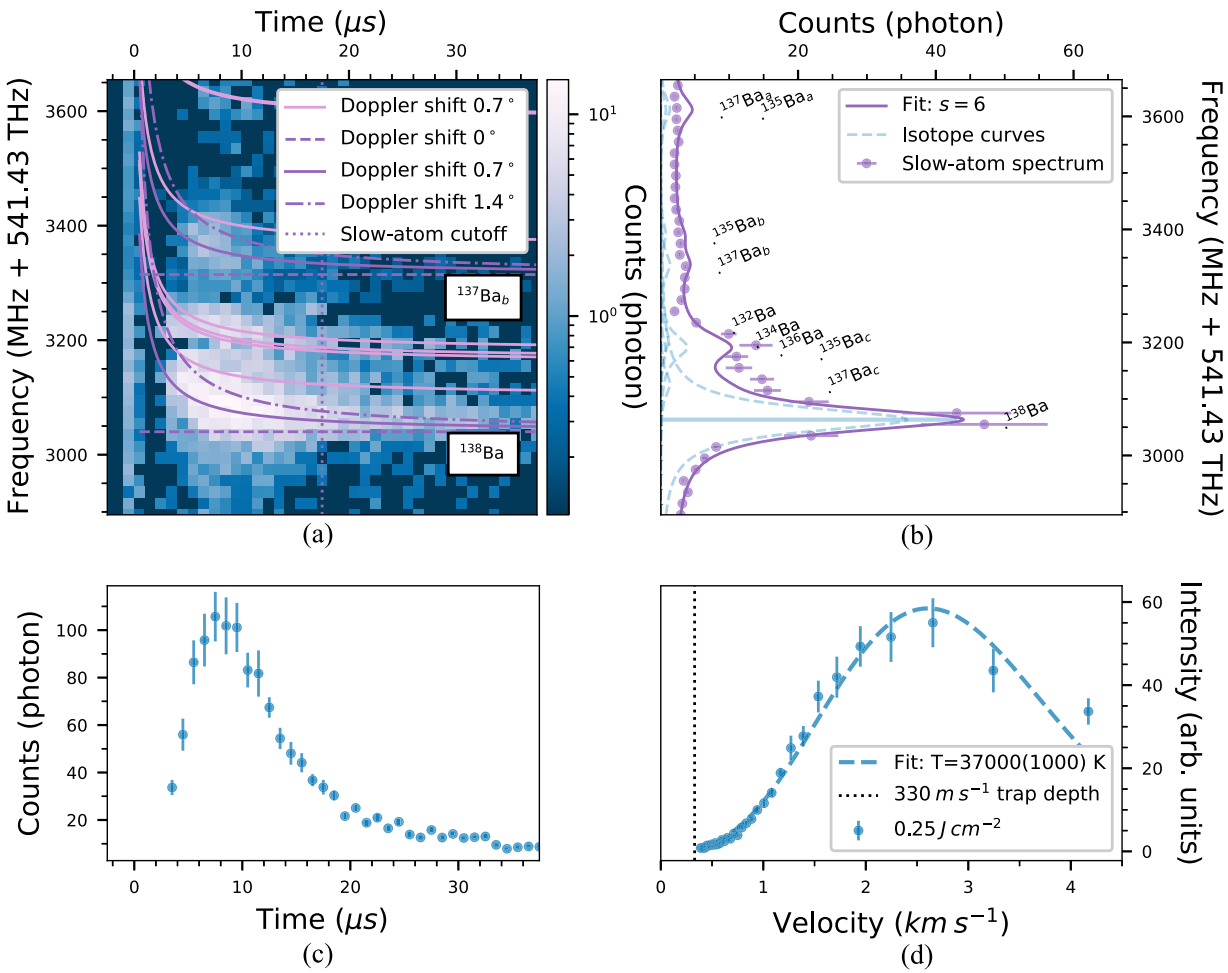

FIG. 4. Time-resolved spectroscopy. First-step photoionization laser power $12 \times P_{\mathrm{sat}}$, ablation fluence $0.25\,\mathrm{J/cm^2}$. (a) Neutral fluorescence collected from our natural-abundance target for different first-step photoionization frequencies and time-window starts. Two spots on the target were used for the data sets with the second spot used for $f \geqslant 3315$ MHz. Doppler shifts for a range of angles 0–1.7° are shown (relevant transitions ^{138}Ba and ^{137}Ba are purple and others in pink) with the fit curves as solid lines. The dotted-purple line denotes the boundary for slow atoms used to generate (b). (b) First-step photoionization spectrum from integrating over the times for slow atoms in (a) [50,61,62]. Subscripts on isotopes denote different transitions; (a)–(c) denote $J' = 1/2, 3/2, 5/2$, respectively (see Table I). (c) Overall time-of-flight distribution from integrating over all frequencies in (a). (d) Velocity distribution generated by scaling the time-of-flight data in (c) appropriately and converting to velocity (see the text). The dotted line indicates the highest velocity an atom can be trapped with, based on our estimation of trap depth (see the Supplemental Material [69]).

control for the temporally varying signal. For the calibration steps, the laser frequency is set to the ^{138}Ba peak, and a 55-μs time window is used, starting at 2.5 μs after the ablation pulse. Photons collected in time bins closer to the moment of the laser pulse come from faster atoms in the ablation plume.

Only slow atoms with a lower kinetic energy than the trap depth can be confined in the Paul trap. From the full time-resolved spectrum, the first-step photoionization spectrum for slow atoms is generated as shown in Fig. 4(b). Most isotopes' peaks are distinguishable, including the well-isolated ^{137}Ba ($J' = 3/2$) peak we use for trapping this isotope. A fit is performed using the known theoretical transition frequencies, transition strengths of different barium isotopes [61,62,64], and the isotopic abundances.

Integrating the time-resolved spectrum over frequency results in the time-resolved distribution in Fig. 4(c). Using the fixed distance from the ablation target to the trap center $d = 14.6$ mm and scaling by $1/\tau$, where τ is the time after the ablation pulse (to account for the transit time through the imaging- system field of view), results in the velocity distribution in Fig. 4(d). A Maxwell-Boltzmann distribution,

$$f_v(\tau) = \frac{A}{\tau} e^{-(md^2)/(2\tau^2 k_b T)} \tag{1}$$

is fit to extract a plume temperature of 37 000 (1000) K. Here, A is an amplitude-scaling parameter, v is the atom velocity, m is the average mass of natural-abundance barium, and k_B is the Boltzmann constant. The peak velocity of the distribution is 2 600(50) $\mathrm{ms^{-1}}$.

If the first-step photoionization laser were perfectly perpendicular to the ablation plume, one would expect the laser frequency to have a global influence on the brightness in the time-resolved spectroscopy data. In the case where the two are an angle θ off from perpendicular, high-velocity atoms

see the laser frequency Doppler shifted. Therefore, the peak frequency for different speeds of ions are Doppler shifted as follows:

$$f_{ob} = f_s\left(1 + \frac{d\ \sin\ \theta}{c\tau}\right), \tag{2}$$

where f_s is the laser frequency and c is the speed of light. A two-dimensional fit to the time-resolved spectrum is performed using this model in conjunction with Eq. (1) and the model used to describe the spectrum in Fig. 4(b) (see the Supplemental Material [69]). The Doppler shifts resulting from this fit are shown as the black and green curves in Fig. 4(a) with a fit angle of $\theta = 0.7^\circ$. For this data set, the specific spots on the ablation target were $\sim$200 μm from the target center. Assuming the ablation target and first-step photoionization laser are well aligned to the viewport axes, the angle between the atomic beam and the laser is $\sim 1^\circ$, very near the fit result of 0.7°.

V. ION LOADING AND SELECTIVITY

With a reliable source of neutral barium, it is straightforward to photoionize and confine ions within the trap. To pick a specific isotope of barium, the 554-nm laser frequency is parked on the desired peak in Fig. 4(b). The 405-nm laser then fully ejects a valence electron of the selected isotope, resulting in an ion confined within the pseudopotential well of our trap. If the kinetic energy of the ionized barium is below the trap depth potential, it will remain within the well. Cooling laser beams at 493 and 650 nm with frequency configuration depending on the chosen isotope cool newly confined ions until they become crystallized within a small area at the center of the trap. In this section, we present results for the loading rates and selectivities for both ^{138}Ba$^+$ and the less-abundant isotope ^{137}Ba$^+$.

We define the loading rate as the average number of ions trapped for each ablation pulse. Using a first-step photoionization-laser saturation of $s = 150$, the loading rate for ^{138}Ba$^+$ is measured to be very close to 1 ion/pulse (out of 20 pulses). Using the same parameters, the ^{137}Ba$^+$ loading rate is measured to be 0.1 ion/pulse (out of 53 pulses), very close to the expected loading rate based on comparing isotopic abundances and transition strengths between the two isotopes.

A dual-bandpass filter is used in our imaging system, allowing for measurement of both neutral-atom fluorescence during ablation and ion fluorescence of trapped ions. We observe that the neutral-fluorescence signal of slow atoms, measured after the slow-atom cutoff in Fig. 4(a), is well correlated with the loading rate (see the Supplemental Material [69]). Using this correlation, the expected loading rate can be actively monitored without needing to perform a statistical trapping experiment.

To quantify the ability to choose isotopes using the two-step photoionization method, we define the selectivity $p_{\rm sel}$ as the probability of loading an isotope. We also define $p_{\rm nat}$ as the natural selectivity, given by the isotope's natural abundance. We further define the selectivity enhancement as

$$\varepsilon_{\rm sel} = \ln\left(\frac{p_{\rm sel}}{1 - p_{\rm sel}}\right) - \ln\left(\frac{p_{\rm nat}}{1 - p_{\rm nat}}\right). \tag{3}$$

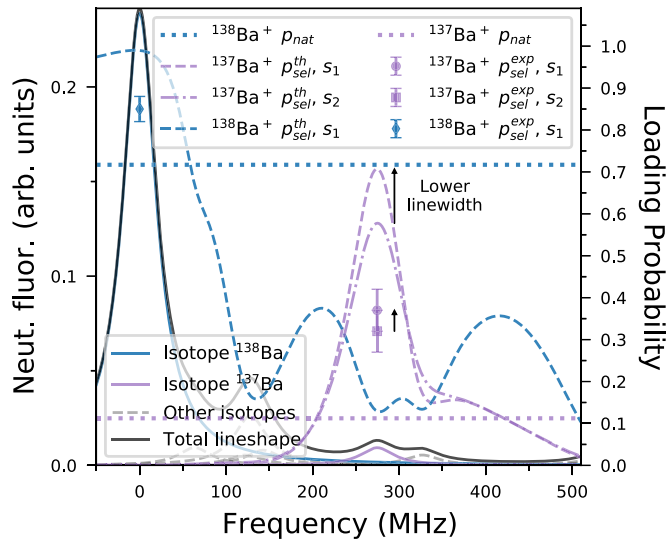

FIG. 5. Selectivity of ^{137}Ba$^+$. Theoretical loading probabilities for isotopes of barium using two-step photoionization $p^{\rm th}_{\rm sel}$ are calculated by comparing their Gaussian curves to the total line shape. Experimentally measured $p^{\rm exp}_{\rm sel}$ are shown as points. s_1 and s_2 denote 5× and 10× saturations, respectively.

Here, each natural logarithm is the logit function. This measure compares an achieved selectivity to the selectivity for a unbiased loading method, which traps according to an isotopes' $p_{\rm nat}$. A selectivity enhancement of zero corresponds to no selectivity, and a selectivity enhancement of near one is roughly a halving of the number of unwanted isotopes compared to the desired isotope. In our setup, we have the ability to discriminate between all naturally abundant isotopes of barium except for ^{135}Ba$^+$. In order to measure the percent of desired ions loaded, considering all trapped atomic or molecular ions, chains of ^{137}Ba$^+$ are trapped and the number of bright ^{137}Ba$^+$ ions is compared to the number of dark ions. In Fig. 5, the expected theoretical selectivities for ^{138}Ba$^+$ and ^{137}Ba$^+$ are shown as a function of the first-step photoionization laser frequency, and for different saturations of the transition (i.e., different transition linewidths). The experimentally measured selectivities are also shown in this figure with the ^{137}Ba$^+$ selectivity enhancement increasing from $\varepsilon = 1.3$ to $\varepsilon = 1.5$ by lowering the transition linewidth, and ^{138}Ba$^+$ giving a selectivity enhancement of $\varepsilon = 0.8$. In all cases, the achieved selectivity is lower than the theoretical. However for ^{137}Ba$^+$, the selectivity does improve with a lower transition linewidth as expected.

No isotope-selective loading experiments were performed with the low-volume ablation target, owing to the inability to reliably produce neutral atoms.

VI. CONCLUSIONS

Many of the observations about the varying neutral-fluorescence signal can be explained by the result that the majority of atomic flux is directed perpendicular to the surface of the ablation target [70–72]. Due to this effect, if the surface normal vector of a spot on the target is unsuitably shaped, atomic-flux density directed through the trap center is

expected to be lower. We hypothesize that conditioning a spot or an area changes the surface profile, transforming the shape to be more suitably directed towards the trap center in addition to the common belief that conditioning serves to purge away a surface layer of contaminants [25,31].

Others groups have opined that temporal reduction of neutral-fluorescence signal is the result of an extreme-pitting process where the severely angled ablation laser has dug a hole into the target such that the ablated spot no longer has line of sight to the center of the trap [26,32,73]. However, Ref. [31] showed that for calcium-metal targets, the depth of pitting from ablation using low-pulse fluence is negligible. Since we see no visible difference in a used spot on our target, we instead suspect the temporal reduction is due to a less severe surface-profile change. We see further evidence towards this explanation (see the Supplemental Material [69]), but whether these effects are from a changing surface geometry is uncertain at this point.

The time-resolved spectroscopy results indicate that plume temperatures from ablating the barium-salt targets are high, at around 37 000 K. Most other groups have measured a neutral-atom ablation plume temperature of 1000 to 10 000 K [24,33,58], but some have measured similar temperatures as us [58,74]. Our barium-salt target could be exhibiting different plume dynamics, or the contrast may partly be explained by a difference in data analysis. In order to take into account Doppler shift, a time-resolved distribution should be collected over a spectrum as performed in this paper and Ref. [58]. If the distribution is only collected for one frequency and Doppler shift is present, the velocity distribution will appear to give a lower temperature.

During data collection, we calibrate the wavelength of the 553-nm laser to the first-step photoionization $^{138}Ba^+$ peak before every experiment (including the selectivity experiment). We perform a frequency scan, collecting slow-atom neutral fluorescence (with a collection window starting 17 μs after the ablation pulse with a 55-μs width). The calibration helps alleviate slow drifts in the measured peak frequency, which we attribute to the wavelength meter used for locking the laser, but because of Doppler shift, the found peak may be up to 10 MHz from the actual peak.

As shown in Fig. 5, we were unable to achieve the expected selectivity for $^{137}Ba^+$. One mechanism that may be affecting selectivity for this isotope is charge exchange [51,52,55,75]. When trying to trap more ions, an already selectively trapped $^{137}Ba^+$ ion can experience an electron-transfer collision,

$$^{137}\overset{+}{\mathrm{Ba}} + {}^{138}\mathrm{Ba} \rightarrow {}^{137}\mathrm{Ba} + {}^{138}\overset{+}{\mathrm{Ba}}, \tag{4}$$

resulting in a trapped-$^{138}Ba^+$ ion instead. Because of its relatively large abundance, this charge exchange is likely to result in more $^{138}Ba^+$ trapped, reducing the selectivity of other isotopes. Mortensen *et al.* [75] demonstrated this effect strikingly, using it to swap out most of a large crystal of $^{44}Ca^+$ ions with the much more abundant $^{40}Ca^+$ isotope.

Another observation is that our selectivity enhancement for $^{138}Ba^+$ was lower than for $^{137}Ba^+$ (i.e., it was less selective). During selective trapping of $^{138}Ba^+$, our Doppler cooling lasers also cool the other unwanted even isotopes, making them easier to be accidentally trapped. This effect could be causing this reduction in the selectivity enhancement compared to for $^{137}Ba^+$.

One simple method of improving selectivity, if only one isotope is needed, is to acquire an isotope-enriched target. However, often more than one of the isotopes are used in an experiment. In addition, current techniques used to source $^{133}Ba^+$ targets leave equal amounts of $^{132}Ba^+$ and $^{133}Ba^+$ with no further separation, so the other selectivity techniques are still needed. To improve on the photoionization presented in this paper, a different photoionization path could be employed with the first step of photionization exciting to the $6\,^3P_1$ state using a 791-nm laser [19,20,22]. This scheme has larger isotope shifts and has already been used to selectively load $^{137}Ba^+$ ions [20]. Other methods have been employed to improve selectivity further by postloading distillation [51,55,76–80]. These methods involve heating the unwanted isotope out of the trap using either the cooling lasers [51,55,76–78] or by applying an additional rf to the trap, exciting the secular motion [79,80].

We demonstrated that the low-density radioactive target is unsuitable for producing neutral-barium atoms with laser ablation, owing to the short timescale on which spots are depleted. Our observed lifetime for neutral-atom production is many orders of magnitude shorter than that measured in Refs. [14,81] for direct Ba^+ ion production. We further observe evidence that our lifetime for direct-ion production (described in the Supplemental Material [69]) is significantly shorter than that seen in Refs. [14,81]. We observed in separate experiments that melting and recrystallizing the $BaCl_2$ before ablation, which was performed in Refs. [14,81] but not in our paper, improves the mechanical integrity of a $BaCl_2$ layer; we hypothesize that a high-temperature treatment may extend the lifetime of direct-ion production from $BaCl_2$ either by adhering the salt to its substrate more securely or by impregnating some of the barium atoms deeper into the substrate [81,82]. Future work is needed to develop a reliable source for neutral ^{133}Ba atoms.

ACKNOWLEDGMENTS

This research was supported, in part, by the Natural Sciences and Engineering Research Council of Canada (NSERC), RGPIN-2018-05253 and the Canada First Research Excellence Fund (CFREF) (Transformative Quantum Technologies), CFREF-2015-00011.

[1] L. M. Duan and C. Monroe, Colloquium: Quantum networks with trapped ions, Rev. Mod. Phys. **82**, 1209 (2010).

[2] C. D. Bruzewicz, J. Chiaverini, R. McConnell, and J. M. Sage, Trapped-ion quantum computing: Progress and challenges, Appl. Phys. Rev. **6**, 021314 (2019).

[3] C. Ospelkaus, U. Warring, Y. Colombe, K. R. Brown, J. M. Amini, D. Leibfried, and D. J. Wineland, Microwave quantum logic gates for trapped ions, Nature (London) **476**, 181 (2011).

[4] M. R. Dietrich, N. Kurz, T. Noel, G. Shu, and B. B. Blinov, Hyperfine and optical barium ion qubits, Phys. Rev. A **81**, 052328 (2010).

[5] C. J. Ballance, T. P. Harty, N. M. Linke, M. A. Sepiol, and D. M. Lucas, High-Fidelity Quantum Logic Gates Using Trapped-Ion Hyperfine Qubits, Phys. Rev. Lett. **117**, 060504 (2016).

[6] J. P. Gaebler, T. R. Tan, Y. Lin, Y. Wan, R. Bowler, A. C. Keith, S. Glancy, K. Coakley, E. Knill, D. Leibfried, and D. J. Wineland, High-Fidelity Universal Gate Set for $^{9}Be^{+}$ Ion Qubits, Phys. Rev. Lett. **117**, 060505 (2016).

[7] Y. Shapira, R. Shaniv, T. Manovitz, N. Akerman, and R. Ozeri, Robust Entanglement Gates for Trapped-Ion Qubits, Phys. Rev. Lett. **121**, 180502 (2018).

[8] A. E. Webb, S. C. Webster, S. Collingbourne, D. Bretaud, A. M. Lawrence, S. Weidt, F. Mintert, and W. K. Hensinger, Resilient Entangling Gates for Trapped Ions, Phys. Rev. Lett. **121**, 180501 (2018).

[9] J. E. Christensen, D. Hucul, W. C. Campbell, and E. R. Hudson, High-fidelity manipulation of a qubit enabled by a manufactured nucleus, npj Quantum Inf. **6**, 35 (2020).

[10] C. J. Ballance, V. M. Schäfer, J. P. Home, D. J. Szwer, S. C. Webster, D. T. C. Allcock, N. M. Linke, T. P. Harty, D. P. L. Aude Craik, D. N. Stacey, A. M. Steane, and D. M. Lucas, Hybrid quantum logic and a test of Bell's inequality using two different atomic isotopes, Nature (London) **528**, 384 (2015).

[11] T. R. Tan, J. P. Gaebler, Y. Lin, Y. Wan, R. Bowler, D. Leibfried, and D. J. Wineland, Multi-element logic gates for trapped-ion qubits, Nature (London) **528**, 380 (2015).

[12] C. D. Bruzewicz, R. McConnell, J. Stuart, J. M. Sage, and J. Chiaverini, Dual-species, multi-qubit logic primitives for Ca^{+}/Sr^{+} trapped-ion crystals, npj Quantum Inf. **5**, 102 (2019).

[13] A. C. Hughes, V. M. Schäfer, K. Thirumalai, D. P. Nadlinger, S. R. Woodrow, D. M. Lucas, and C. J. Ballance, Benchmarking of a high-fidelity mixed-species entangling gate, Phys. Rev. Lett. **125**, 080504 (2020).

[14] D. Hucul, J. E. Christensen, E. R. Hudson, and W. C. Campbell, Spectroscopy of a Synthetic Trapped Ion Qubit, Phys. Rev. Lett. **119**, 100501 (2017).

[15] P. J. Low, B. M. White, A. A. Cox, M. L. Day, and C. Senko, Practical trapped-ion protocols for universal qudit-based quantum computing, Phys. Rev. Research **2**, 033128 (2020).

[16] N. Kjærgaard, L. Hornekær, A. M. Thommesen, Z. Videsen, and M. Drewsen, Isotope selective loading of an ion trap using resonance-enhanced two-photon ionization, Appl. Phys. B: Lasers Opt. **71**, 207 (2000).

[17] S. Gulde, D. Rotter, P. Barton, F. Schmidt-Kaler, R. Blatt, and W. Hogervorst, Simple and efficient photo-ionization loading of ions for precision ion-trapping experiments, Appl. Phys. B: Lasers Opt. **73**, 861 (2001).

[18] R. G. DeVoe and C. Kurtsiefer, Experimental study of anomalous heating and trap instabilities in a microscopic ^{137}Ba ion trap, Phys. Rev. A **65**, 063407 (2002).

[19] A. V. Steele, L. R. Churchill, P. F. Griffin, and M. S. Chapman, Photoionization and photoelectric loading of barium ion traps, Phys. Rev. A **75**, 053404 (2007).

[20] B. Wang, J. W. Zhang, C. Gao, and L. J. Wang, Highly efficient and isotope selective photo-ionization of barium atoms using diode laser and LED light, Opt. Express **19**, 16438 (2011).

[21] G. Leschhorn, T. Hasegawa, and T. Schaetz, Efficient photo-ionization for barium ion trapping using a dipole-allowed resonant two-photon transition, Appl. Phys. B: Lasers Opt. **108**, 159 (2012).

[22] R. D. Graham, S.-P. Chen, T. Sakrejda, J. Wright, Z. Zhou, and B. B. Blinov, A system for trapping barium ions in a microfabricated surface trap, AIP Adv. **4**, 057124 (2014).

[23] T. G. Ballance, J. F. Goodwin, B. Nichol, L. J. Stephenson, C. J. Ballance, and D. M. Lucas, A short response time atomic source for trapped ion experiments, Rev. Sci. Instrum. **89**, 053102 (2018).

[24] G. Vrijsen, Y. Aikyo, R. F. Spivey, I. V. Inlek, and J. Kim, Efficient isotope-selective pulsed laser ablation loading of $^{174}Yb^{+}$ ions in a surface electrode trap, Opt. Express **27**, 33907 (2019).

[25] S. Olmschenk and P. Becker, Laser ablation production of Ba, Ca, Dy, Er, La, Lu, and Yb ions, Appl. Phys. B: Lasers Opt. **123**, 99 (2017).

[26] R. D. Knight, Storage of ions from laser-produced plasmas, Appl. Phys. Lett. **38**, 221 (1981).

[27] R. E. Russo, Laser ablation, Appl. Spectrosc. **49**, 14A (1995).

[28] P. R. Willmott and J. R. Huber, Pulsed laser vaporization and deposition, Rev. Mod. Phys. **72**, 315 (2000).

[29] M. N. R. Ashfold, F. Claeyssens, G. M. Fuge, and S. J. Henley, Pulsed laser ablation and deposition of thin films, Chem. Soc. Rev. **33**, 23 (2004).

[30] C. Phipps, *Laser Ablation and Its Applications* (Springer, Berlin, 2007), Vol. 129.

[31] R. J. Hendricks, D. M. Grant, P. F. Herskind, A. Dantan, and M. Drewsen, An all-optical ion-loading technique for scalable microtrap architectures, Appl. Phys. B: Lasers Opt. **88**, 507 (2007).

[32] D. R. Leibrandt, R. J. Clark, J. Labaziewicz, P. Antohi, W. Bakr, K. R. Brown, and I. L. Chuang, Laser ablation loading of a surface-electrode ion trap, Phys. Rev. A **76**, 055403 (2007).

[33] K. Sheridan, W. Lange, and M. Keller, All-optical ion generation for ion trap loading, Appl. Phys. B: Lasers Opt. **104**, 755 (2011).

[34] S. J. Schowalter, K. Chen, W. G. Rellergert, S. T. Sullivan, and E. R. Hudson, An integrated ion trap and time-of-flight mass spectrometer for chemical and photo- reaction dynamics studies, Rev. Sci. Instrum. **83**, 043103 (2012).

[35] Y. Hashimoto, L. Matsuoka, H. Osaki, Y. Fukushima, and S. Hasegawa, Trapping laser ablated Ca^{+} ions in linear Paul trap, Jpn. J. Appl. Phys., Part 1 **45**, 7108 (2006).

[36] D. A. Davies, D. J. Morrissey, G. Bollen, P. A. Lofy, J. Ottarson, and S. C. Schwarz, A high-power laser ablation ion source for Penning trap studies of nuclear reaction products, J. Phys.: Conf. Ser. **59**, 136 (2007).

[37] K. Zimmermann, M. V. Okhapkin, O. A. Herrera-Sancho, and E. Peik, Laser ablation loading of a radiofrequency ion trap, Appl. Phys. B: Lasers Opt. **107**, 883 (2012).

[38] A. Poschl, Laser ablation loading and single ion addressing of strontium in a linear paul trap, Ph.D. thesis, Royal Institute of Technology in Stockholm, 2018.

[39] M. Sameed, D. Maxwell, and N. Madsen, Ion generation and loading of a Penning trap using pulsed laser ablation, New J. Phys. **22**, 013009 (2020).

[40] M. Niemann, T. Meiners, J. Mielke, M. J. Borchert, and J. M. Cornejo, Cryogenic be penning trap for precision cryogenic $^{9}Be^{+}$ penning trap for precision measurements with (anti-)protons, Meas. Sci. Technol. **31**, 035003 (2020).

[41] V. H. S. Kwong, Production and storage of low-energy highly charged ions by laser ablation and an ion trap, Phys. Rev. A **39**, 4451 (1989).

[42] L. Láska, K. Jungwirth, B. Králiková, J. Krása, M. Pfeifer, K. Rohlena, J. Skála, J. Ullschmied, J. Badziak, P. Parys, J. Wolowski, E. Woryna, S. Gammino, L. Torrisi, F. P. Boody, and H. Hora, Generation of multiply charged ions at low and high laser-power densities, Plasma Phys. Control. Fusion **45**, 585 (2003).

[43] T. Kwapień, U. Eichmann, and W. Sandner, Sympathetic cooling of laser-produced doubly charged ions in a few-ion crystal, Phys. Rev. A **75**, 063418 (2007).

[44] C. J. Campbell, A. V. Steele, L. R. Churchill, M. V. DePalatis, D. E. Naylor, D. N. Matsukevich, A. Kuzmich, and M. S. Chapman, Multiply Charged Thorium Crystals for Nuclear Laser Spectroscopy, Phys. Rev. Lett. **102**, 233004 (2009).

[45] O. Kornienko, P. T. A. Reilly, W. B. Whitten, and J. M. Ramsey, Electron impact ionization in a microion trap mass spectrometer, Rev. Sci. Instrum. **70**, 3907 (1999).

[46] O. J. Orient and A. Chutjian, A compact, high-resolution Paul ion trap mass spectrometer with electron-impact ionization, Rev. Sci. Instrum. **73**, 2157 (2002).

[47] K. R. Brown, R. J. Clark, J. Labaziewicz, P. Richerme, D. R. Leibrandt, and I. L. Chuang, Loading and characterization of a printed-circuit-board atomic ion trap, Phys. Rev. A **75**, 015401 (2007).

[48] M. Cetina, A. Grier, J. Campbell, I. Chuang, and V. Vuletić, Bright source of cold ions for surface-electrode traps, Phys. Rev. A **76**, 041401(R) (2007).

[49] C. G. Gill, A. W. Garrett, P. H. Hemberger, and N. S. Nogar, Selective laser ablation/ionization for ion trap mass spectrometry: Resonant laser ablation, Spectrochim. Acta, Part B **51**, 851 (1996).

[50] K. Yamada, N. Ozaki, M. Yamamoto, and K. I. Ueyanagi, Separation of barium isotopes by selective two-step photoionization process, J. Nucl. Sci. Technol. **25**, 641 (1988).

[51] D. M. Lucas, A. Ramos, J. P. Home, M. J. McDonnell, S. Nakayama, J.-P. Stacey, S. C. Webster, D. N. Stacey, and A. M. Steane, Isotope-selective photoionization for calcium ion trapping, Phys. Rev. A **69**, 012711 (2004).

[52] U. Tanaka, H. Matsunishi, I. Morita, and S. Urabe, Isotope-selective trapping of rare calcium ions using high-power incoherent light sources for the second step of photo-ionization, Appl. Phys. B: Lasers Opt. **81**, 795 (2005).

[53] C. Balzer, A. Braun, T. Hannemann, C. Paape, M. Ettler, W. Neuhauser, and C. Wunderlich, Electrodynamically trapped Yb^{+} ions for quantum information processing, Phys. Rev. A **73**, 041407(R) (2006).

[54] M. Brownnutt, V. Letchumanan, G. Wilpers, R. C. Thompson, P. Gill, and A. G. Sinclair, Controlled photoionization loading of $^{88}Sr^{+}$ for precision ion-trap experiments, Appl. Phys. B: Lasers Opt. **87**, 411 (2007).

[55] U. Tanaka, I. Morita, and S. Urabe, Selective loading and laser cooling of rare calcium isotope $^{43}Ca^{+}$, Appl. Phys. B: Lasers Opt. **89**, 195 (2007).

[56] C. Schuck, M. Almendros, F. Rohde, M. Hennrich, and J. Eschner, Two-color photoionization of calcium using SHG and LED light, Appl. Phys. B: Lasers Opt. **100**, 765 (2010).

[57] M. Johanning, A. Braun, D. Eiteneuer, C. Paape, C. Balzer, W. Neuhauser, and C. Wunderlich, Resonance-enhanced isotope-selective photoionization of YbI for ion trap loading, Appl. Phys. B: Lasers Opt. **103**, 327 (2011).

[58] M. Guggemos, D. Heinrich, O. A. Herrera-Sancho, R. Blatt, and C. F. Roos, Sympathetic cooling and detection of a hot trapped ion by a cold one, New J. Phys. **17**, 103001 (2015).

[59] J. Zhang, Y. Xie, P.-f. Liu, B.-q. Ou, W. Wu, and P.-x. Chen, Realizing three-step photoionization of calcium by two lasers, Appl. Phys. B: Lasers Opt. **123**, 45 (2017).

[60] H. Shao, M. Wang, M. Zeng, H. Guan, and K. Gao, Laser ablation and two-step photo-ionization for the generation of $^{40}Ca^{+}$, J. Phys. Commun. **2**, 095019 (2018).

[61] P. E. G. Baird, R. J. Brambley, K. Burnett, D. N. Stacey, D. M. Warrington, G. K. Woodgate, and H. G. Kuhn, Optical isotope shifts and hyperfine structure in 553.5 nm of barium, Proc. R. Soc. London, Ser. A **365**, 567 (1979).

[62] K. Bekk, A. Andl, S. Göring, A. Hanser, G. Nowicki, H. Rebel, and G. Schatz, Laserspectroscopic studies of collective properties of neutron deficient Ba Nuclei, Z. Phys. A: At. Nucl. **291**, 219 (1979).

[63] S. Niggli and M. C. Huber, Transition probabilities in neutral barium, Phys. Rev. A **35**, 2908 (1987).

[64] W. A. van Wijngaarden and J. Li, Hyperfine splittings and isotope shifts of $(6s)^{2}{}^{1}s_0 \rightarrow (6s6p)^{1}p_1$ transition in barium, Can. J. Phys. **73**, 484 (1995).

[65] D. Kulaga, J. Migdalek, and O. Bar, Transition probabilities and lifetimes in neutral barium, J. Phys. B: At., Mol. Opt. Phys. **34**, 4775 (2001).

[66] P. J. Low, Tolerable experimental imperfections for a quadrupole blade ion trap and practical qudit gates with trapped ions, Ph.D. thesis, University of Waterloo, 2019.

[67] B. M. Bramman, Measuring trapped ion qudits, Ph.D. thesis, University of Waterloo, 2019.

[68] Selectivity ablation data, https://doi.org/10.5281/zenodo.6029079 (2022).

[69] See Supplemental Material at http://link.aps.org/supplemental/10.1103/PhysRevA.105.033102 for more details on the experiments and results presented and smaller results which guided the main results.

[70] L. Láska, J. Krása, M. Pfeifer, K. Rohlena, S. Gammino, L. Torrisi, L. Andò, and G. Ciavola, Angular distribution of ions emitted from Nd:YAG laser-produced plasma, Rev. Sci. Instrum. **73**, 654 (2002).

[71] B. Thestrup, B. Toftmann, J. Schou, B. Doggett, and J. G. Lunney, Ion dynamics in laser ablation plumes from selected metals at 355 nm, Appl. Surf. Sci. **197-198**, 175 (2002).

[72] L. Láska, K. Jungwirth, J. Krása, E. Krouský, M. Pfeifer, K. Rohlena, A. Velyhan, J. Ullschmied, S. Gammino, L. Torrisi, J. Badziak, P. Parys, M. Rosinski, L. Ryć, and J. Wolowski, Angular distributions of ions emitted from laser plasma produced at various irradiation angles and laser intensities, Laser Part. Beams **26**, 555 (2008).

[73] D. B. Chrisey, *Pulsed Laser Deposition of Thin Films* (Wiley, New York, 1994), Vol. 1, Chap. 4.

[74] J. B. Matos, M. G. Destro, C. A. B. Silveira, and N. A. S. Rodrigues, Neutral atomic jet generation by laser ablation of copper targets, Rev. Sci. Instrum. **85**, 083505 (2014).

[75] A. Mortensen, J. J. T. Lindballe, I. S. Jensen, P. Staanum, D. Voigt, and M. Drewsen, Isotope shifts of the $4s^{21}S_0 \rightarrow 4s5p^1P_1$ transition and hyperfine splitting of the $4s5p^1P_1$ state in calcium, Phys. Rev. A **69**, 042502 (2004).

[76] K. Toyoda, H. Kataoka, Y. Kai, A. Miura, M. Watanabe, and S. Urabe, Separation of laser-cooled $_{42}$Ca+ and $_{44}$Ca+ in a linear Paul trap, Appl. Phys. B: Lasers Opt. **72**, 327 (2001).

[77] M. Kitaoka and S. Hasegawa, Isotope-selective manipulation of Ca^+ using laser heating and cooling in a linear Paul trap, J. Phys. B: At., Mol. Opt. Phys. **45**, 165008 (2012).

[78] P. V. Borisyuk, S. P. Derevyashkin, K. Y. Khabarova, N. N. Kolachevsky, Y. Y. Lebedinsky, S. S. Poteshin, A. A. Sysoev, A. V. Tkalya, D. O. Tregubov, V. I. Troyan, O. S. Vasiliev, V. P. Yakovlev, and V. I. Yudin, Mass selective laser cooling of $^{229}Th^{3+}$ in a multisectional linear paul trap loaded with a mixture of thorium isotopes, Eur. J. Mass Spectrometry **23**, 136 (2017).

[79] R. Alheit, K. Enders, and G. Werth, Isotope separation by nonlinear resonances in a Paul trap, Appl. Phys. B: Lasers Opt. **62**, 511 (1996).

[80] T. Hasegawa and T. Shimizu, Removal of irrelevant isotope ions in the presence of laser cooling in a rf trap, Appl Phys B: Lasers Opt. **70**, 867 (2000).

[81] J. E. Christensen, High-fidelity operation of a radioactive trapped ion qubit, ^{133}Ba, Ph.D. thesis, University of California, Los Angeles, 2020.

[82] D. Laughlin and K. Hono, *Physical Metallurgy* (Elsevier, Amsterdam, 2015), Vol. 1, Chap. 5.